
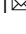


Increasing risks of extreme salt intrusion events across European estuaries in a warming climate

Jiyong Lee¹  , Bouke Biemond¹, Huib de Swart¹ & Henk A. Dijkstra¹

Over the last decade, many estuaries worldwide have faced increased salt intrusion as a result of human activities and a changing climate. Despite its socio-economic importance, our current projections on the statistics of future salt intrusion are limited to case studies in certain regions. Here, we show that, compared to present-day conditions, river discharge in the summer months is projected to be reduced by 10–60% in 17 out of 22 investigated major European river basins at the end of the 21st century under the high CO₂ emission scenario (Shared Socioeconomic Pathways, SSP 3-7.0). We find that the reduced future river discharge in the summer months, in turn, increases salt intrusion lengths by 10–30% in 9 representative European estuaries at low and mid latitudes. Our analysis further indicates that the European estuaries are projected to experience more than five times more frequent extreme salt intrusion events.

¹Institute for Marine and Atmospheric research Utrecht (IMAU), Utrecht University, Princetonplein 5, Utrecht 3584 CC, The Netherlands. email: j.lee3@uu.nl

Estuaries are the semi-enclosed bodies of water between river and open sea, where saline and fresh water mix. Estuaries provide unique socio-economic and ecological environments that support diverse species and human communities. An important aspect of an estuary is its subtidal salinity distribution, which is the result of salt import by estuarine circulation and tidal pumping, and salt export by river flow. The extent of salt intrusion in an estuary is quantified by a salt intrusion length, here defined as the distance of the 2- ψ isohaline to the estuary mouth (X_2)¹. Earlier studies focusing on isolated individual estuaries have shown that saline water will be intruded further inland in the coming decades due to extended drought periods², sea level rise³, anthropogenic land subsidence⁴, and channel deepening⁵. Extreme salt intrusion events cause severe problems associated with drinking water supplies and food production, resulting in huge economic losses^{3,6,7}. Thus, there is an urgent need for reliable decadal time scale projections of salt intrusion in estuaries to develop better mitigation and adaptation strategies.

Among the future changes in external climate forcing (sea level rise, river discharge, tides, waves, and many others), particular attention has been given to decreasing upstream freshwater discharge⁸. In a warming climate, spatio-temporal patterns of precipitation, evapotranspiration, and snowmelt are projected to change, which results in significant variability in freshwater availability on the land surfaces^{9–11}. While some projections have assessed future freshwater availability at continental or global scales^{12–14}, there has been little attention to connecting macro-hydrological modeling outcomes with salt intrusion processes in estuaries.

Only a few studies exist in which detailed three-dimensional surface water hydrodynamic numerical models were used to provide regional scale projections of salt intrusion under specific future climate scenarios^{2,4,8}. However, most of those earlier work focused on one realization of each future climate variable for the salt intrusion projection due to the high computational costs. As a result, quantifying uncertainties in statistics of future salt intrusion, associated with climate variability, was infeasible. In addition, those studies were often limited to a single location to keep the analysis manageable. Hence, we currently lack an understanding on the statistics of projected salt intrusion lengths beyond isolated individual estuaries.

In this paper, we quantify relative changes of 35-year mean and return periods of extreme events for future salt intrusion in estuaries located across the European continent. Hereafter, the extreme salt intrusion events correspond to 1 in 100-year occurrence during the summer months in the present climate (1996–2030). The extreme salt intrusion events are considered as cases in which saline ocean water is intruded far more upstream inland than usual, jeopardizing low-lying coastal communities. We first determine daily freshwater discharge for 22 major European river basins at the end of the 21st century under the high CO₂ emission scenario, SSP 3-7.0, using the Community Earth System Model 2 large ensemble simulation results (CESM-LE2)¹⁵, (see Methods and Supplementary Table S1). CESM-LE2 is the only climate model ensemble that provides daily river discharge with a sufficiently large number of members for robust future river projections up to the year 2100. CESM-LE2 was carried out only for the SSP 3-7.0 emission scenario due to large computational costs. The choice of SSP 3-7.0 in CESM-LE2 aligns with the guidance provided by the Coupled Model Inter-comparison Project Phase 6 (CMIP6)¹⁶. Although CESM-LE2 shows comparable results with observational data (Supplementary Fig. S1), the modeled river discharge is corrected using Quantile Delta Mapping (QDM) to avoid systematic biases (see Methods, Supplementary Note S1, and Fig. S2). The time series of observed river discharge are sufficiently long, in a sense that they

show converged Cumulative Distribution Functions (CDFs) (see Supplementary Fig. S3). It is inferred that the bias correction is independent of lengths of the timeseries of the observed river discharge. Comparison of probability density functions between the bias corrected and observed daily river discharge are given in Supplementary Fig. S4.

Next, from these 22 river basins, we select 9 partially (or well) mixed estuaries, for which observed salt intrusion lengths have been reported in the literature^{17–26}. The reasons behind selecting 9 estuaries are associated with avoiding complex estuary configurations and strongly stratified systems, in which the salt intrusion length model in this paper cannot accurately capture physical processes (Methods). For these estuaries, the statistics of present and projected future salt intrusion lengths are determined using a time-dependent deterministic model^{27–29}, see Methods. The reported salt intrusion lengths in the literature are used to determine eddy viscosity and diffusion in this model^{17–26} (Methods and Supplementary Table S2). The calibrated model determines the time-averaged salt intrusion lengths during the observation periods with errors less than 100 m compared to medians of the reported range in the literature (Supplementary Note S2).

Our results show that, as compared to present-day conditions, summer month river discharge is projected to be decreased by 10–60% in 17 out of 22 explored European river basins at the end of the 21st century under SSP 3-7.0. We also find that the reduced future summer month river discharge is expected to increase salt intrusion lengths by 10–30% in the 9 selected European estuaries. Such increased salt intrusion lengths can lead to more than five times more frequent extreme events in the coming decades.

Results

River discharge projection. Large spatial variability is found in the projected relative changes in 35-year mean river discharge $\Delta Q^* = (Q_f - Q_p)/Q_p$ across Europe (Fig. 1). Here, Q_f and Q_p are the time-averaged future (2066–2100) and present (1996–2030) river discharge, respectively. Hereafter, we present ensemble-averaged ΔQ^* from CESM-LE2 unless otherwise specified. A significant decrease in river discharge ($-0.5 \leq \Delta Q^* \leq -0.2$) is projected for estuaries in Southern Europe. A smaller reduction of river discharge ($-0.2 \leq \Delta Q^* \leq 0$) is projected in most western, central, and eastern European countries at mid latitudes. We further find that river discharge will slightly increase ($0 \leq \Delta Q^* \leq 0.1$) in most regions in the United Kingdom (UK) and in Northern Europe.

Figure 2a shows ΔQ^* for the 22 selected river basins, ordered according to their latitude. Uncertainties in the projections are quantified by the standard deviation among climate model ensemble members (black solid lines). Significant decreases (up to ~50%) and moderate increases (up to ~10%) are found in ΔQ^* at low and high latitudes, respectively. For most of the river basins at mid latitudes, the sign of ΔQ^* (increase or decrease) is uncertain due to the large variability in the climate model ensemble (the lengths of the black solid lines are greater than the lengths of the horizontal bars). The trends we find are consistent with those that were obtained from the assessment of the future global water availability, based on the runoff outputs from multiple CMIP5 models⁹.

When we consider the 35-year mean relative changes in the river discharge during only the summer months (June, July, and August), denoted as ΔQ_{JJA}^* , a significant reduction is observed in most of the major European river basins (Fig. 2b). For instance, the river basins at low latitudes show $\Delta Q_{JJA}^* \simeq -0.6$ (60% decrease). The magnitudes in ΔQ_{JJA}^* overall reduce with latitude, resulting in $\Delta Q_{JJA}^* \simeq -0.1$ (10% decrease) in Glomma (Norway).

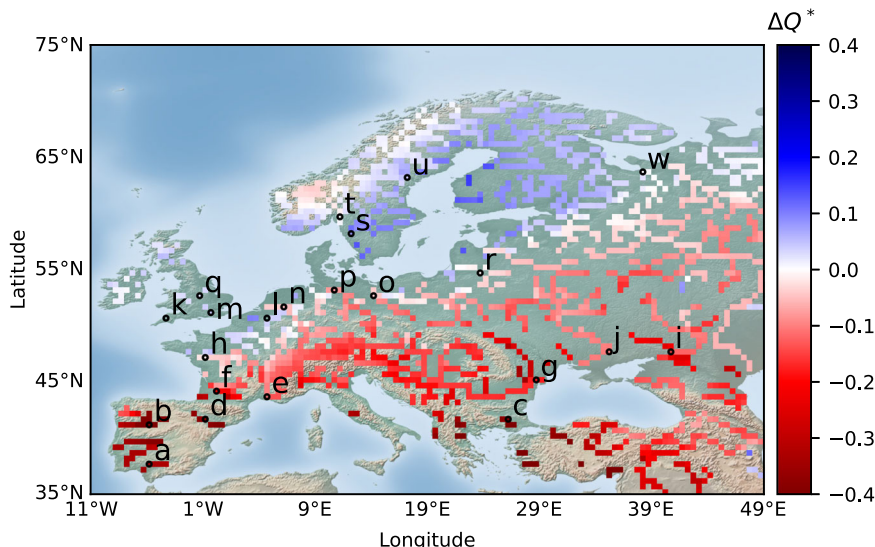


Fig. 1 A map showing the relative changes in the future 35-year mean river discharge with respect to the present condition under the SSP 3-7.0 scenario in CESM-LE2 (see Methods), defined as $\Delta Q^* = (Q_f - Q_p)/Q_p$. Here, Q_f and Q_p are the time-averaged future (2066-2100) and present (1996-2030) river discharge. Only grid cells whose the time-averaged $Q_p \geq 50 \text{ m}^3\text{s}^{-1}$ are presented. The black circles indicate locations where the freshwater discharge is extracted from CESM-LE2 at the outlets of the selected European river basins: (a) Guadalquivir, (b) Douro, (c) Maritsa, (d) Ebro, (e) Rhone, (f) Gironde, (g) Danube, (h) Loire, (i) Don, (j) Dnieper, (k) Tamar, (l) Scheldt, (m) Thames, (n) Rhine-Meuse, (o) Oder, (p) Elbe, (q) Humber, (r) Nemunas, (s) Gota, (t) Glomma, (u) Angermanalven, and (w) Onega.

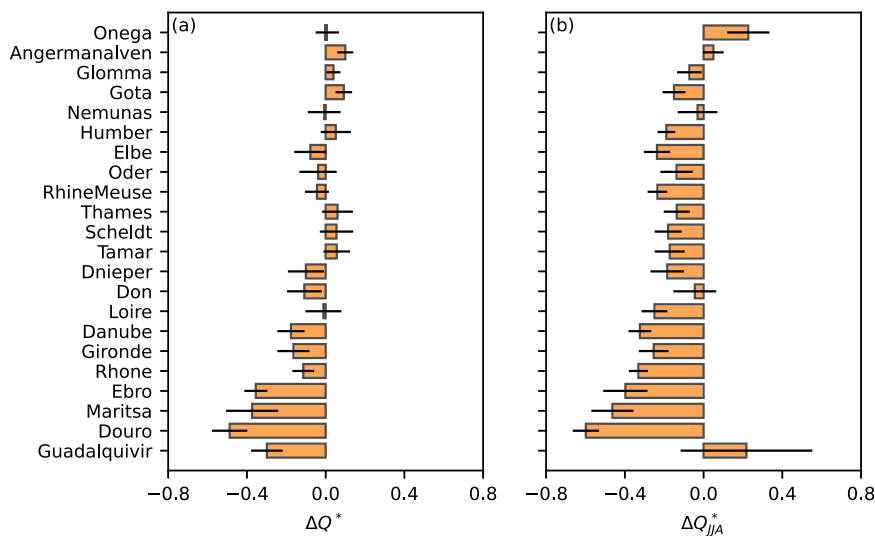


Fig. 2 The relative changes in the 35-year mean river discharge in the future (2066-2100) with respect to the present time (1996-2030) under the SSP 3-7.0 scenario in CESM-LE2. The black horizontal lines indicate uncertainties in the future projections (standard deviation among model ensemble members). Here, the subscript JJA represents June, July, and August. The ordering along the vertical axis corresponds to the ascending latitudes. **a** The resulting future relative changes when all months are considered. **b** The same as **a** but when only the summer months are considered.

Notably, Guadalquivir (Spain) shows an uncertain direction of the river discharge projection with a large ensemble climate variability. This uncertainty is associated with the extremely low river discharge during the summer months in this estuary, which increases the sensitivity of the future river discharge projection (Supplementary Fig. S5a). The positive ΔQ_{JJA}^* in Onega (Russia) is found to be related to enhanced surface and ground runoff during the summer months.

Salt intrusion length projection. With the projected river discharge from CESM-LE2, we calculate the salt intrusion length for 9 partially (or well) mixed estuaries using a time-dependent salt transport model²⁸ (Methods). The relative changes of 35-year

mean in the subtidal (tidally averaged) salt intrusion length are computed with respect to present-day values, for both the entire year (ΔX_2^* , Fig. 3a) and only the summer months ($\Delta X_{2,JJA}^*$, Fig. 3b). The parameter $\Delta X_{2,JJA}^*$ is considered as a representative salt intrusion length for low flows in all the explored river basins. The low flow periods are marked with vertical red-shaded areas in Supplementary Fig. S5. Our results clearly indicate that the salt intrusion length is projected to increase during the summer months in most European estuaries at low and mid latitudes (Fig. 3b). For the Loire, Tamar, Thames, RhineMeuse, and Elbe Estuaries, the increase of salt intrusion length is much larger in the summer months than that considered for the whole year. This is due to enhanced seasonality in the river discharge at the end of

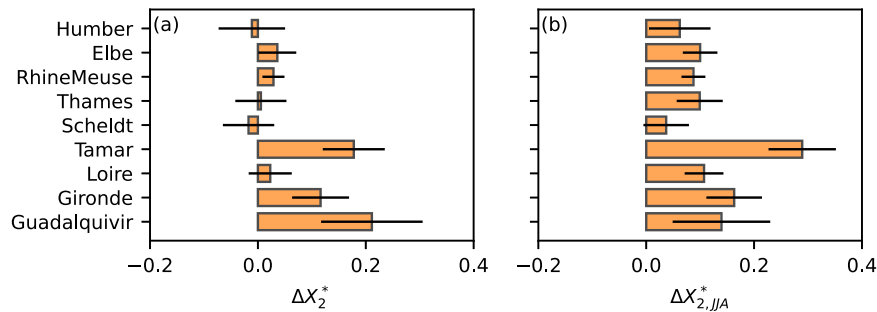


Fig. 3 The relative changes in the 35-year mean salt intrusion length in the future (2066–2100) with respect to the present time (1996–2030) under the SSP 3-7.0 scenario in CESM-LE2. The black horizontal lines indicate uncertainties in the future projection (standard deviation among model ensemble members). Here, $\Delta X_2^* = (X_{2,f} - X_{2,p})/X_{2,p}$, $X_{2,f}$ is the time-averaged future salt intrusion length projection (2066–2100) and $X_{2,p}$ is the time-averaged present salt intrusion length (1996–2030). The subscript JJA represents June, July, and August. The ordering along the vertical axis corresponds to the ascending latitudes. **a** The resulting future relative changes when all months are considered. **b** The same as **a** but when only the summer months are considered.

the 21st century (Supplementary Fig. S5). Such enhanced seasonality will make those estuaries become fresher (or more saline) during periods of high (or low) flow. For the Gironde Estuary, the differences between $\Delta X_{2,JJA}^*$ and ΔX_2^* are less distinct, since the future river discharge will monotonically decrease during the whole year (Supplementary Fig. S5f). For the Guadalquivir Estuary, the summer month river discharge is consistently low both under the present and future climate, while substantial reduction in future river discharge is observed in other months (Supplementary Fig. S5a). This results in smaller $\Delta X_{2,JJA}^*$ as compared to ΔX_2^* .

Besides ΔX_2^* and $\Delta X_{2,JJA}^*$, the changes in the return periods of extreme events are an important statistical parameter for salt intrusion management. Since those that occur 1 in 100-year are conventionally computed from timeseries of annual maxima (or minima), annual summer month mean river discharge (Q_{JJA}^A) and salt intrusion length ($X_{2,JJA}^A$) are analyzed hereafter. We take the Tamar Estuary as an example for demonstrating the shifts in probability density of Q_{JJA}^A and $X_{2,JJA}^A$, and changes in the return periods in the future. The reason to select the Tamar Estuary (UK) is that the largest increase in $\Delta X_{2,JJA}^*$ is found in Fig. 3b. We use Kernel Density Estimation (KDE) functions for visualizing the probability density. In our analysis, KDE is generated based on a Gaussian kernel and bin widths are determined using a grid search method³⁰. Figure 4a shows that Q_{JJA}^A and $X_{2,JJA}^A$ are decreasing and increasing with time, respectively (the ensemble average of the Pearson correlation coefficient is -0.72 ± 0.07 , inferring significant negative correlations). Such trends create shifts in the probability density functions of river discharge and salt intrusion length in future with respect to the ones in present (Fig. 4b, c). Notably, more flattened probability density functions are generated during the future periods. This implies that larger variability is projected for the river discharge and the salt intrusion length in a warming climate.

Next, we compute the return period curves of $X_{2,JJA}^A$ using the Generalized Extreme Value (GEV) theory³¹, see Methods. The generic probability distribution function for the extreme events is computed by the first-order statistics (mean and standard deviation) of $X_{2,JJA}^A$. The parameters in the GEV distributions are fitted using the maximum likelihood method³². Figure 4d demonstrates how the return period curves are projected to change at the end of the 21st century as compared to the present time. We find that the future return periods that correspond to the extreme event (1 in 100-year $X_{2,JJA}^A$ event in the present climate) is reduced to ~ 3 years in the Tamar Estuary.

The same analysis was conducted for the other selected estuaries except Scheldt and Humber. The reason to exclude Scheldt and Humber is that the modeled river discharge before the bias correction has too low variability to accurately compute the return periods (Supplementary Fig. S1m, q). Standard deviations of the seasonal average of the modeled river discharge show less than 25% of those in the observed one in Scheldt and Humber. We find that the return periods of the extreme salt intrusion events in the future also substantially decrease for the remaining estuaries: Guadalquivir (~ 4 years), Gironde (~ 9 years), Loire (~ 42 years), Thames (~ 41 years), RhineMeuse (~ 4 years), and Elbe (~ 12 years). This indicates that events considered as extreme of present would occur more frequently in the future in most of the explored partially (or well) mixed European estuaries.

Discussion

Our study presents the continental-scale salt intrusion projections across Europe at the end of the 21st century under the high CO₂ emission scenario (SSP 3-7.0) using CESM-LE2. Particular attention was given to the summer months, when the extreme salt intrusion events are most likely to occur. We showed that the future 35-year mean of the river discharge during the summer months is projected to be reduced substantially between 10–60% in most major European river basins (Fig. 2b). Using the time-dependent salt intrusion model and GEV analysis, we found that the 35-year mean salt intrusion length is projected to increase 10–30% (Fig. 3) and the extreme events are projected to occur more than five times more frequently than today across the selected European estuaries (Fig. 4d) at the end of the 21st century. Note that we assumed that changes in river discharge are dominant in causing salt intrusion length changes, providing the lower bounds of salt intrusion projections under the high CO₂ emission scenario. In a warming climate, changes in salt intrusion length are not only caused by changes in river discharge, but also by increasing water depth in estuaries due to sea level rise³³.

Although the model used in this paper was developed to study how salt intrusion processes respond to changes in river discharge, the effects of mean sea level rise on salt intrusion are estimated in Supplementary Fig. S6. Based on the fifth Intergovernmental Panel on Climate Change (IPCC) assessment report³⁴, we chose a global mean sea level rise of 0.74 m under the high CO₂ emission scenario (Representative Concentration Pathways, RCP 8.5). A constant sea level rise is assumed over the considered future period (2066–2100). This analysis shows that

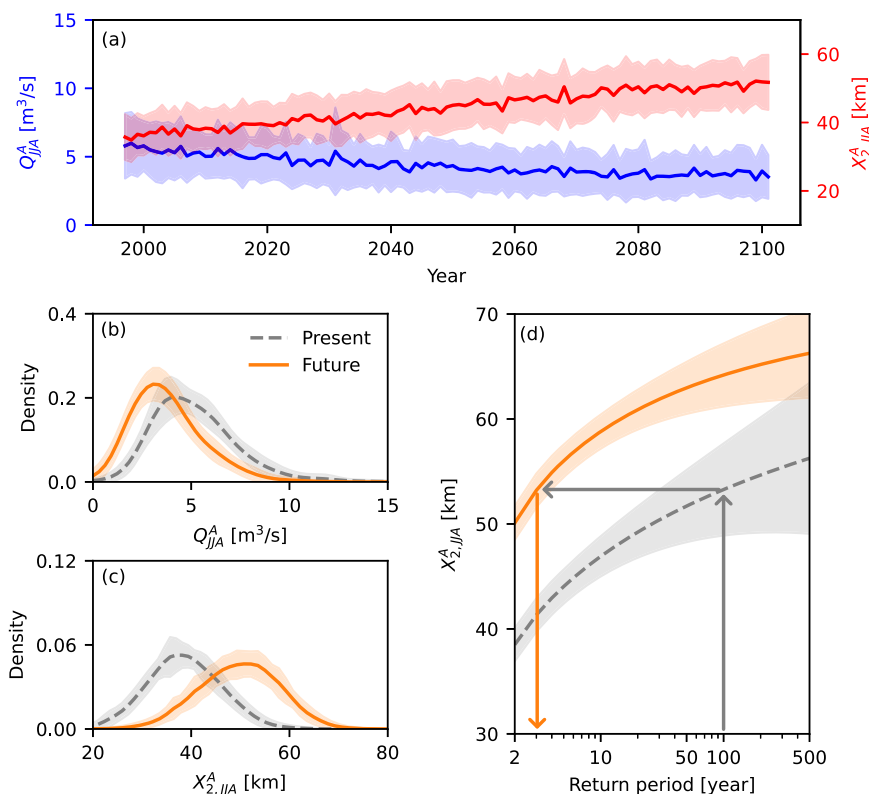


Fig. 4 Future projections of the river discharge and salt intrusion length for the Tamar estuary (UK). **a** Annual mean of summer month river discharge (Q_{JJA}^A , blue) and salt intrusion length ($X_{2,JJA}^A$, red), respectively. **b** Kernel Density Estimation functions from Q_{JJA}^A for the present (1996–2030) and future conditions (2066–2100). **c** Similar to **b** but for $X_{2,JJA}^A$. **d** Return periods of $X_{2,JJA}^A$, where the gray vertical arrow is 1 in 100-year event in the present time, defined as the extreme event. The orange vertical arrow is the reduced return period in the future corresponding to the extreme event. In **a–d**, colored lines show the ensemble-averaged values. The corresponding shaded areas indicate standard deviation among model ensemble members.

the relative importance of sea level rise with respect to changes in river discharge can become comparable for most of the mid latitude estuaries (e.g., Loire, Scheldt, RhineMeuse, Elbe, and Humber).

It is important to stress that regional differences in sea level change are not considered here, which requires much more detailed analysis. Furthermore, the salt intrusion length model we use considers a constant cross-sectional area along an estuary. Thus, increases in water depth result in underestimation of the river flow advection ($-Q/A$) and overestimation of the magnitude of the exchange flow ($C_i, i = 1, 2, 3$) in Eq. (1). Consequently, the model overestimates the impact of mean sea level rise on future salt intrusion. To alleviate such overestimates, we only considered the sea level rise impacts on the exchange flow. It was assumed that reduced river flow velocity is compensated by increased Stokes return velocity with increasing water depth. More sophisticated salt intrusion models need to be used for more accurate quantification of the sea level rise impacts on the future salt intrusion. Quantifying regional differences in sea level changes and accurate contribution of sea level rise to changes in salt intrusion length is beyond the scope of our analysis. For this reason, our analysis on the effects of the sea level rise on salt intrusion needs to be considered as crude estimates.

Saline ocean water is also more likely to be intruded further inland at the end of the 21st century because of the changing statistics of storm surges, and by changes in the tides in shelf seas induced by the sea level rise^{35,36}. In addition, as human populations grow, estuary geometry will be continuously modified by channel deepening for ship navigation⁵, sediment starvation-induced river bed incision, or land subsidence due to excessive groundwater extraction⁴. Moreover, our analysis is centered on

the high CO₂ emission scenario (SSP 3-7.0) due to data constraints. Thus, the above mentioned additional climatic and anthropogenic stressors under various emission scenarios need to be further quantified in the future for the improvement of the salt intrusion projections.

This study focused on the 9 representative partially (or well) mixed European estuaries for salt intrusion length projections. However, the framework we propose can be straightforwardly applied to any other partially (or well) mixed estuaries with given key parameters (e.g. river discharge, estuary geometries, tidal current amplitude, and salt intrusion length). Therefore, our methodology serves as a valuable tool for assessing the first-order macro-scale salt intrusion length projections, which can be used to determine where we need more comprehensive analysis. Discussions should be initiated including stakeholders and experts in various fields (e.g. policy makers, residents, earth scientists, engineers, ecologists, and many more) to prepare climate-proof salt intrusion mitigation and adaptation strategies. A wide range of research from socio-economics, estuary dynamics, to new engineering technology need to be conducted to find solutions for mitigating salt intrusion problems in a warming climate.

Methods

CESM. CESM is a fully coupled global climate model that resolves ocean, atmospheric, land, sea-ice processes, and their interactions. The analysis in this study is based on the CESM2 large ensemble simulation results, CESM-LE2 ($n = 69$), under the Shared Socioeconomic Pathways (SSP) 3-7.0 scenario. Here, n is the total number of ensembles used in our analysis. Representing the amount of radiative forcing by the year 2100 (Wm^{-2}), the SSP3-7.0 scenario is the medium to high end of future forcing. All

the simulations were conducted with 1° nominal horizontal spatial resolution for periods 1850–2100 and the future forcing was applied from 2015. CESM-LE2 is part of CMIP6 and full descriptions about the project are available at <https://www.cesm.ucar.edu/community-projects/lens2>.

CESM2 is an improved version of CESM1³⁷. Among many others, there has been an advancement in the river routing scheme, which is important for the specific purpose of this study. In CESM1, the water is assumed to be transported with the constant effective flow velocity across the globe³⁸. Instead in CESM2, spatially varying flow velocities are allowed using Manning's equation with different representative roughness, hydraulic radius, and water surface slopes in land grid cells^{39,40}.

Bias correction. Although the modeled river discharges by CESM-LE2 agree well with those observed in most of the selected river basins, systematic under- or over-estimations are observed in some river basins (Supplementary Fig. S1). To avoid biases in the salt intrusion analysis, we corrected the modeled river discharge time series using Quantile Delta Mapping (QDM)⁴¹. The main idea behind QDM is to compute statistical difference in cumulative distribution functions (CDF) of climate variables between reference (observation) and projection time periods in a simulation. Thereafter, the statistical differences in the simulations are mapped on CDFs of the observational data (Supplementary Fig. S2). We ensure that CDFs of the observed river discharge data are statistically converged (Supplementary Fig. S3). The advantage of this bias correction method is that trends in future projection in simulations are preserved, while obtaining accurate representation in the historical time. Detailed mathematical descriptions of QDM and its sensitivity on the modeled river discharge are elaborated in Supplementary Note 1.

Salt intrusion length. Salt intrusion length is calculated using a time-dependent idealized sub-tidal model²⁸. The model is based on cross-sectionally averaged equations for hydrodynamics and the salt budget²⁷, and the governing equation reads:

$$\frac{1}{2} \frac{dX}{dt} = -\frac{Q}{A} + \frac{C_3}{X^3} + \frac{Q C_2}{A X^2} + \left(\frac{Q}{A}\right)^2 \frac{C_1}{X} + \frac{C_0}{X}. \quad (1)$$

Here, X [m] is the distance from the mouth of an estuary to a location where salinity vanishes, Q [m^3s^{-1}] is the prescribed river discharge (from CESM-LE2 or observation data in this study), and A [m^2] is the cross-sectional area of the estuary (assumed constant). Furthermore, C_i , $i = 0, 1, 2, 3$ are the positive coefficients associated with eddy viscosity and diffusion. The model assumes a linearly decreasing depth-averaged salinity from the mouth of the estuary. Thus, lengths to the conventional critical salinity ($s_2 = 2$ psu) are calculated from $X_2 = (1 - s_2/s_{ocn})X$. The ocean salinity s_{ocn} is assumed to be 35 psu. On the right-hand side of the equation, the first term describes the decrease in salt intrusion length by freshwater influx. The second, third, and fourth terms represent increases in salt intrusion length by vertical eddy mixing due to exchange flow. The last term is increase in saltwater intrusion by tidal dispersion. The fourth-order Runge-Kutta scheme is used for the numerical time integration and temporal resolutions of the daily river discharge timeseries are increased by linearly interpolating to 0.5–4 hourly signals to ensure the stability and the convergence of numerical solutions. We used constant coefficients associated with eddy viscosity and diffusion (C_i , $i = 0, 1, 2, 3$) under the entire range of river discharge conditions, including both spring and neap tides. It was ensured that the statistics of the relative changes in salt intrusion length from the model are robust and do not depend on whether time-dependent or different eddy viscosity and diffusivity are

used. Details about the coefficients associated with eddy viscosity and diffusion are given in the Supplementary Note S2.

Down-selection of estuaries for salt intrusion projections. Among the 22 river basins, we focus on the 9 partially (or well) mixed estuaries for salt intrusion projections. We first exclude estuaries that are highly stratified due to weak tidal actions, in which two-layer flows occur (e.g., Ebro, Rhone, Maritsa, Danube, Dnieper, and Don). We also exclude estuaries with complex configurations. For example, Oder and Nemunas have a large body of water (i.e., lagoon) in-between main freshwater channels and estuary mouths. Glomma, Gota, and Angermanalven have multiple outlets separated by several islands near their mouths. Onega is not included in the analysis because it has different cycles of hydrological projections.

Return periods. We compute return periods from $X_{2/JJA}^A$. The open source Python package *genextreme.py* is used to fit the Generalized Extreme Value (GEV) theory³¹ and compute the return periods. Despite of its simplicity, the return period has been used in different research fields to determine the likelihood of extreme events and assess the corresponding risks⁴². The generic probability density function is defined as:

$$F(Z^*) = e^{-(1-\zeta Z^*)^{\frac{1}{\lambda}}(1-\zeta Z^*)^{\frac{1}{\lambda}-1}}, \quad (2)$$

where, $Z^* = (X_2 - \lambda)/\sigma$. In Eq. (2), the parametric constants (ζ , λ , and σ) represent the shape, location, and scale of the distributions, respectively. The parametric constants (ζ , λ , and σ) of the fitted distribution are determined based on the maximum likelihood method³². The parameters (λ and σ) are associated with the mean and standard deviation of the fitted distributions and given data. The fitted GEV distributions are compared with the KDE functions and histograms from the input data samples, showing good agreement (Supplementary Fig. S7).

Data availability

The observed daily river discharge used in the analysis of this paper can be downloaded from <https://www.chguadalquivir.es/saih/Inicio.aspx> (Guadalquivir), <http://www.hydro.eaufrance.fr> (Gironde), <https://www.waterinfo.be/Meetrekesen> (Scheldt), and <https://portal.grdc.bafg.de/> (the rest of the river basins). Names of river discharge measurement stations are listed in Table S1. The observed salinity data for the Loire estuary can be also downloaded from <https://www.loire-estuaire.org/>.

Code availability

All the scripts to reproduce processed data and the figures presented in this paper are available at <https://zenodo.org/records/10451480>.

Received: 14 June 2023; Accepted: 16 January 2024;

Published online: 31 January 2024

References

1. Monismith, S. G., Kimmerer, W., Burau, J. R. & Stacey, M. T. Structure and flow-induced variability of the subtidal salinity field in northern San Francisco Bay. *J. Phys. Oceanogr.* **32**, 3003–3019 (2002).
2. Rodrigues, M., Fortunato, A. B. & Freire, P. Saltwater intrusion in the upper Tagus Estuary during droughts. *Geosciences* **9**, 400 (2019).
3. Smajgl, A. et al. Responding to rising sea levels in the Mekong Delta. *Nat. Clim. Change* **5**, 167–174 (2015).
4. Eslami, S. et al. Projections of salt intrusion in a mega-delta under climatic and anthropogenic stressors. *Commun. Earth Environ.* **2**, 142 (2021).
5. Ralston, D. K. & Geyer, W. R. Response to channel deepening of the salinity intrusion, estuarine circulation, and stratification in an urbanized estuary. *J. Geophys. Res. Oceans* **124**, 4784–4802 (2019).
6. Ferguson, G. & Gleeson, T. Vulnerability of coastal aquifers to groundwater use and climate change. *Nat. Clim. Change* **2**, 342–345 (2012).

7. Zhu, J. et al. Dynamic mechanism of an extremely severe saltwater intrusion in the Changjiang Estuary in February 2014. *Hydrol. Earth Syst. Sci.* **24**, 5043–5056 (2020).
8. Bellafiore, D. et al. Saltwater intrusion in a Mediterranean delta under a changing climate. *J. Geophys. Res. Oceans* **126**, e2020JC016437 (2021).
9. Koirala, S., Hirabayashi, Y., Mahendran, R. & Kanae, S. Global assessment of agreement among streamflow projections using CMIP5 model outputs. *Environ. Res. Lett.* **9**, 064017 (2014).
10. Prudhomme, C. et al. Hydrological droughts in the 21st century, hotspots and uncertainties from a global multimodel ensemble experiment. *Proc. Natl Acad. Sci.* **111**, 3262–3267 (2014).
11. Konapala, G., Mishra, A. K., Wada, Y. & Mann, M. E. Climate change will affect global water availability through compounding changes in seasonal precipitation and evaporation. *Nat. Commun.* **11**, 3044 (2020).
12. Nohara, D., Kitoh, A., Hosaka, M. & Oki, T. Impact of climate change on river discharge projected by multimodel ensemble. *J. Hydrometeorol.* **7**, 1076–1089 (2006).
13. Hirabayashi, Y., Kanae, S., Emori, S., Oki, T. & Kimoto, M. Global projections of changing risks of floods and droughts in a changing climate. *Hydrol. Sci. J.* **53**, 754–772 (2008).
14. van Vliet, M. T. et al. Global river discharge and water temperature under climate change. *Global Environ. Change* **23**, 450–464 (2013).
15. Rodgers, K. B. et al. Ubiquity of human-induced changes in climate variability. *Earth Syst. Dyn.* **12**, 1393–1411 (2021).
16. O'Neill, B. C. et al. The scenario model intercomparison project (ScenarioMIP) for CMIP6. *Geosci. Model Dev.* **9**, 3461–3482 (2016).
17. Van Der Burgh, I. P. Prediction of the extent of saltwater intrusion into estuaries and seas. *J. Hydraul. Res.* **6**, 267–288 (1968).
18. Uncles, R. & Stephens, J. The freshwater-saltwater interface and its relationship to the turbidity maximum in the Tamar Estuary, United Kingdom. *Estuaries* **16**, 126–141 (1993).
19. Friedrichs, C. T. & Aubrey, D. G. Tidal propagation in strongly convergent channels. *J. Geophys. Res. Oceans* **99**, 3321–3336 (1994).
20. Cave, R. R. et al. The Humber catchment and its coastal area: from UK to European perspectives. *Sci. Total Environ.* **314**, 31–52 (2003).
21. Prandle, D. Saline intrusion in partially mixed estuaries. *Estuarine Coastal Shelf Sci.* **59**, 385–397 (2004).
22. Diez-Minguito, M., Contreras, E., Polo, M. & Losada, M. Spatio-temporal distribution, along-channel transport, and post-riverflood recovery of salinity in the Guadalquivir Estuary (SW Spain). *J. Geophys. Res. Oceans* **118**, 2267–2278 (2013).
23. Gisen, J., Savenije, H. & Nijzink, R. Revised predictive equations for salt intrusion modelling in estuaries. *Hydrol. Earth Syst. Sci.* **19**, 2791–2803 (2015).
24. Naithani, J. et al. An ecological model for the Scheldt Estuary and tidal rivers ecosystem: spatial and temporal variability of plankton. *Hydrobiologia* **775**, 51–67 (2016).
25. van Maanen, B. & Sottolichio, A. Hydro-and sediment dynamics in the Gironde Estuary (France): Sensitivity to seasonal variations in river inflow and sea level rise. *Cont. Shelf Res.* **165**, 37–50 (2018).
26. Robins, P. E. et al. Improving estuary models by reducing uncertainties associated with river flows. *Estuarine Coastal Shelf Sci.* **207**, 63–73 (2018).
27. MacCready, P. Estuarine adjustment. *J. Phys. Oceanogr.* **37**, 2133–2145 (2007).
28. Chen, S.-N. Asymmetric estuarine responses to changes in river forcing: A consequence of nonlinear salt flux. *J. Phys. Oceanogr.* **45**, 2836–2847 (2015).
29. Geyer, W. R. & MacCready, P. The estuarine circulation. *Ann. Rev. Fluid Mech.* **46**, 175–197 (2014).
30. Bishop, C. M. & Nasrabadi, N. M. *Pattern recognition and machine learning*, vol. 4 (Springer, 2006).
31. Jenkinson, A. F. The frequency distribution of the annual maximum (or minimum) values of meteorological elements. *Q. J. R. Meteorol. Soc.* **81**, 158–171 (1955).
32. Smith, R. L. Maximum likelihood estimation in a class of nonregular cases. *Biometrika* **72**, 67–90 (1985).
33. Pein, J., Staneva, J., Mayer, B., Palmer, M. D. & Schrum, C. A framework for estuarine future sea-level scenarios: Response of the industrialised Elbe Estuary to projected mean sea level rise and internal variability. *Front. Marine Sci.* **10**, 1102485 (2023).
34. Pachauri, R. K. et al. Climate change 2014: synthesis report. In *Contribution of Working Groups I, II and III to the fifth assessment report of the Intergovernmental Panel on Climate Change* (IPCC, 2014).
35. Pickering, M. et al. The impact of future sea-level rise on the global tides. *Cont. Shelf Res.* **142**, 50–68 (2017).
36. Muis, S. et al. Global projections of storm surges using high-resolution CMIP6 climate models. *Earths Fut.* **11**, e2023EF003479 (2023).
37. Danabasoglu, G. et al. The community earth system model version 2 (CESM2). *J. Adv. Model. Earth Syst.* **12**, e2019MS001916 (2020).
38. Branstetter, M. L. & Erickson III, D. J. Continental runoff dynamics in the Community Climate System Model 2 (CCSM2) control simulation. *J. Geophys. Res.* **108**, 4550 (2003).
39. Tesfa, T. K. et al. A subbasin-based framework to represent land surface processes in an Earth system model. *Geosci. Model Dev.* **7**, 947–963 (2014).
40. Li, H.-Y. et al. Evaluating global streamflow simulations by a physically based routing model coupled with the community land model. *J. Hydrometeorol.* **16**, 948–971 (2015).
41. Cannon, A. J., Sobie, S. R. & Murdock, T. Q. Bias correction of GCM precipitation by quantile mapping: how well do methods preserve changes in quantiles and extremes? *J. Clim.* **28**, 6938–6959 (2015).
42. AghaKouchak, A. et al. Climate extremes and compound hazards in a warming world. *Ann. Rev. Earth Planet. Sci.* **48**, 519–548 (2020).

Acknowledgements

This work is financially supported by NWO Domain Applied and Engineering Sciences (2022/TTW/01344701) in collaboration with private and public partners. The authors appreciate Dutch National Supercomputer (Snellius) for the computational resources and thankful to Michael Klijhuis for his technical support. We are also grateful to Dr. René Wijngaard and Dr. René van Westen for discussions on the data analysis.

Author contributions

J.L. designed the study, analyzed main results, and led writing of the paper. B.B. contributed to data analysis and reviewed the paper. H.de.S. contributed to data analysis and reviewed the paper. H.A.D. provided financial support and computational resources, contributed to data analysis, and reviewed the paper.

Competing interests

The authors declare no competing interests.

Additional information


Supplementary information The online version contains supplementary material available at <https://doi.org/10.1038/s43247-024-01225-w>.

Correspondence and requests for materials should be addressed to Jiyong Lee.

Peer review information *Communications Earth & Environment* thanks Zhaoqing Yang and the other, anonymous, reviewer(s) for their contribution to the peer review of this work. Primary Handling Editors: Jennifer Veitch, Clare Davis and Heike Langenberg. A peer review file is available.

Reprints and permission information is available at <http://www.nature.com/reprints>

Publisher's note Springer Nature remains neutral with regard to jurisdictional claims in published maps and institutional affiliations.

 **Open Access** This article is licensed under a Creative Commons Attribution 4.0 International License, which permits use, sharing, adaptation, distribution and reproduction in any medium or format, as long as you give appropriate credit to the original author(s) and the source, provide a link to the Creative Commons licence, and indicate if changes were made. The images or other third party material in this article are included in the article's Creative Commons licence, unless indicated otherwise in a credit line to the material. If material is not included in the article's Creative Commons licence and your intended use is not permitted by statutory regulation or exceeds the permitted use, you will need to obtain permission directly from the copyright holder. To view a copy of this licence, visit <http://creativecommons.org/licenses/by/4.0/>.

© The Author(s) 2024